Quantifying the densification and shear flow under indentation deformation in borosilicate glasses

Kasimuthumaniyan, Subramanian; Sahoo, Sourav; Smedskjaer, Morten M.; Krishnan, Naduvath Mana Anoop; Gosvami, Nitya Nand

Published in:
International Journal of Applied Glass Science

DOI (link to publication from Publisher):
10.1111/ijag.16598

Publication date:
2022

Document Version
Accepted author manuscript, peer reviewed version

Quantifying the Densification and Shear Flow under Indentation Deformation in Borosilicate Glasses

S. Kasimuthumaniyan[1], Sourav Sahoo[1], Morten M. Smedskjaer[2], N. M. Anoop Krishnan[3,4,*], Nitya Nand Gosvami[1,*]

[1]Department of Materials Science and Engineering, Indian Institute of Technology Delhi, Hauz Khas, New Delhi 110016, India

[2]Department of Chemistry and Bioscience, Aalborg University, DK-9220 Aalborg, Denmark

[3]Department of Civil Engineering, Indian Institute of Technology Delhi, Hauz Khas, New Delhi 110016, India

[4]School of Artificial Intelligence, Indian Institute of Technology Delhi, Hauz Khas, New Delhi 110016, India

*** Corresponding author:**

E-mail: krishnan@iitd.ac.in (N. M. Anoop Krishnan)

Phone: +91(11)2659-1223 (O)

E-mail: ngosvami@iitd.ac.in (Nitya Nand Gosvami)

Phone: +91(11)2659-6414 (O)

Abstract

Borosilicate glasses are used ubiquitously for a wide range of applications, where their mechanical properties play a critical role. However, the deformation mechanism governing the sharp contact response of these glasses remain poorly understood. Herein, we analyze the

This article has been accepted for publication and undergone full peer review but has not been through the copyediting, typesetting, pagination and proofreading process, which may lead to differences between this version and the Version of Record. Please cite this article as doi: 10.1111/ijag.16598.

role of elasto-plastic response in determining the indentation deformation mechanisms for a range of borosilicate glass compositions. The series of glasses were made by varying the SiO_2 to B_2O_3 molar ratio while maintaining a constant content of network modifying alkali and alkaline earth oxides. We employed nanoindentation followed by annealing below the glass transition temperature to quantify the contribution of densification and shear flow as a function of glass composition. Interestingly, we observe that the volume recovery upon annealing is inversely proportional to the hardness of the glasses. This suggests that the resistance to permanent deformation is closely related to the network connectivity of the glasses, which in turn governs the mechanism of deformation under sharp contact loading. Overall, we show the important role of alkali and alkaline earth modifiers in governing the composition dependent indentation behavior of borosilicate glass series.

1. Introduction

Borosilicate glasses, with boron and silicon as the major network formers along with alkali or alkaline earth modifier species, form a major family of glasses with several commercial applications [1,2]. Such glasses offer high resistance to chemical attack, good glass forming ability, and low coefficient of thermal expansion [1–3]. Owing to these desirable properties, borosilicate glasses are used in laboratory glassware [2,3], household cooking utensils [2], automobile headlamps [2,3], biomedical applications [4], and are a highly preferred candidate for nuclear waste immobilization [5–8]. In addition, borosilicate glasses provide a range of physical and chemical properties with the interaction of alkali and alkaline earth ions with boron and silicon structural units [1–3]. For instance, alkali borosilicates have been used as thermal shock-resistant glasses, whereas alkaline earth borosilicate glasses are used as substrate glasses for liquid crystal displays when also mixed with alumina [1,9]. Understanding the structural origin

of the properties of borosilicate glasses, such as hardness, is also significant in developing improved glass compositions that exhibit higher mechanical strength and scratch resistance wherever contact deformations are involved, for example, pharmaceutical packaging such as syringes, ampoules, and cartridges [10,11].

One of the primary reason why borosilicate glasses exhibit a unique range of properties could be attributed to the well-known "boron anomaly", i.e., the non-monotonic variation in glass properties with composition [1–3]. This anomaly is related to the composition dependent behavior of boron speciation, which takes a coordination number of four or three depending on the availability, or lack, of network modifiers. [1–3,12,13].. Glassy B_2O_3 consists mostly of planar trigonal BO_3 layers. These trigonal layers are connected by bridging oxygens (BO) at their corners and a large fraction of these connect to form three-membered boroxol rings [14]. This structure makes the boron network undergo permanent deformation easier compared to the four-fold coordinated silicate network [1]. However, the presence of network modifiers in the borosilicate glass network acts as charge compensators in increasing the network connectivity rather than the role of breaking the connectivity as in silicate network [1–3]. Specifically, the three-coordinated boron network (B^3) transforms to a four-coordinated boron network (B^4). This charge compensation role of network modifiers acts until the boron anomaly boundary beyond which it plays the role of depolymerizing the silicate/boron network [1,2,14–16]. Several studies, including both computer simulations [17–19] and experimental work [1,13,20,21], confirm this boron speciation transition between three-fold coordinated (trigonal) and four-fold coordinated (tetrahedral) structural motifs with the addition of alkali and alkaline earth network modifiers [22,23], which in turn affect their physical, mechanical, thermal, and optical properties.

Hardness is an important mechanical property of glasses that affect their durability and service lifetime. In addition, hardness is occasionally used as a proxy to understand the scratch or wear resistance of glasses [24]. The ease of operation, sample requirements, and short experimental duration have made the indentation technique popular among glass researchers for measuring glass mechanical properties [25,26]. During the last few decades, the indentation technique has been implemented for measuring various properties such as scratch hardness [24], normal hardness [27], elastic modulus [28], indentation fracture toughness [23], and crack resistance [29], to mention a few. Besides, instrumented indentation technique, such as nanoindentation, is useful for understanding the elasto-plastic behavior of glasses [30]. Researchers have also applied the elasticity data acquired from load-displacement curve for studying the composition dependent mechanical behavior of glasses [31–33]. For instance, Miura et al. [33] have used elastic recovery data obtained from nanoindentation load-displacement curves to reveal the composition-dependent deformation behavior of copper phosphate and silicate-based glasses. Indeed, elasto-plastic data can give indirect insights into the deformation modes of glasses[34].

Typically, during indentation, glasses undergo permanent (plastic) deformation through two major indentation deformation mechanisms, namely densification and shear flow [35,36]. Research in the past revealed that the part of the deformed zone can be recovered through thermal annealing, as the energy required to initiate volume recovery is much lower than the energy required to initiate viscous flow[23]. Later, Yoshida et al. [37] proposed a protocol for quantifying such indentation deformation mechanisms for a variety of glasses by combining microindentation technique with annealing and atomic force microscopy (AFM). Thereafter, this technique has been successfully applied by other glass researchers [14,38–42] for a variety of glass compositions. Although various studies exist in the literature on understanding the

composition-dependent indentation deformation of borosilicate glasses [14,15,21,43,44], these studies focus mostly on ternary alkali borosilicate glass systems.

Specifically, there are very few studies on the indentation deformation mechanisms of quaternary alkali-alkaline earth borosilicate glass series, although these are more prevalent in practical applications, for example, in nuclear waste immobilization applications or pharmaceutical packaging. The quaternary borosilicate series can be considered as the simplest representation of the nuclear waste glass for waste immobilization [45,46]. Further, the presence of the higher field strength alkaline earth Ca^{2+} ions along with Na^{+} may potentially improve the chemical durability[2,47] and mechanical response[48–50] of the quaternary borosilicate glasses.

To address this knowledge gap, we here use nanoindentation technique with Berkovich indenter followed by the annealing protocol to study the composition dependent mechanical behavior of alkali-alkaline earth borosilicate glass series. By analyzing the governing densification and shear flow mechanisms, we show that the glass hardness is inversely proportional to the volume recovery for the alkali-alkaline borosilicate glass compositions used in this study, which, in turn, correlates with the network connectivity. Considering the significance of borosilicate glasses, we believe that the present work may give more insight regarding their structure-hardness relationship toward developing glass composition with improved hardness and strength for practical applications.

2. Experimental details

2. 1 Materials

All the glasses used in the borosilicate series were prepared by traditional melt-quenching technique and annealed at their respective glass transition temperature (T_g) as given in Table

1. In a previous study [1], the fractions of four-coordinated boron (N^4) and silicon with four bridging oxygens (Q^4) were determined using ^{11}B and ^{29}Si magic angle spinning (MAS) NMR spectroscopy, respectively. The elaborate glass preparation procedure and detailed MAS NMR spectra discussions is given elsewhere [1,51]. The compositions of the borosilicate glass series were determined through wet chemical analysis[1,51] using ICP-OES (Inductively coupled plasma - optical emission spectrometry) for which the uncertainty is within ±0.5% (see Table 1). Hereafter, the glasses used in the present study will be recognized by the glass ID as shown in Table 1. The glass series was selected to illustrate a constant network modifier content (Na_2O, CaO) with varying network former ratio (SiO_2/B_2O_3).

2. 2 Sample preparation

The prepared glass bars were wet polished (Buehler, Metaserv, 250, Grinder-Polisher) using ethanol to avoid the glass dissolution [52]. The glass surfaces were successively polished using 400/800/1200 grit size silicon carbide (SiC) emery papers. Then, cloth polishing was performed with grade-1 alumina for at least an hour until the satisfactory surface quality was achieved to proceed with the final cloth polishing step using 0.05 μm alumina suspension (Chennai Metco, India). After cloth polishing, the polished borosilicate glass specimens were ultrasonicated in ethanol for at least 15 mins to remove any surface contaminants associated with polishing. Then, the surfaces were dried using nitrogen gas before the nanoindentation and AFM experiments. To make the surface suitable for these measurements, the average surface roughness (R_a) on a 10×10 μm^2 area measured by contact mode AFM was ensured to be less than 3 nm.

2. 3 Nanoindentation

Nanoindentation measurements were made using a universal nanomechanical tester (ASMEC, Germany). A Berkovich diamond probe having a nominal radius of approximately 300 nm was used. Before the experiment on the borosilicate glass specimens, tip area function and machine compliance were calibrated on the standard fused silica glass specimen with known elastic properties (Young's Modulus E = 72.1 GPa, Poisson's ratio ν = 0.17) as per the well-established Oliver-Pharr method [28]. The observed deviations with respect to the known property (E) of the fused silica glass specimen was around 3-5%. Further, during calibrations the modulus profile obtained using QCSM (quasi continuous stiffness measurement) was not deviating significantly even 30 nm from the surface till the maximum depth of penetration. After ensuring the standard observations, nanoindentation experiments were carried out on the borosilicate glasses. Indentations were performed at a loading rate of 5 mN/s until the defined normal load of 50 mN[31]. The defined maximum load was held constant for a duration of 5 seconds before unloading at 5 mN/s. For all the experimental data, thermal drift correction at a standard rate of 0.1 nm/s was carried out post-indentation. Note that the indentations were performed at least on 5 different locations. Hardness was determined from the load-displacement curve based on the Oliver-Pharr method as [28]:

$$H = \frac{P_{max}}{A_p} \tag{1}$$

where P_{max} is the maximum applied normal load, and A_p is the projected contact area at maximum defined load. The projected contact area A_p is calculated by evaluating an empirical indenter shape function $A_p = f(h_c)$. In this study, as hardness is not an intrinsic material property[31], the bluntness of the tip was not considered in the measurement of hardness. Hence, for an ideal Berkovich indenter,

$$A_p = 24.56\, h_c^2 \quad (2)$$

where h_c is the contact depth between indenter and the glass specimen at P_{max}, which is estimated by using the equation as follows:

$$h_c = h_{max} - \varepsilon \frac{P_{max}}{S} \quad (3)$$

In the above Eq. (3), ε is a geometrical constant (ε = 0.75 for a Berkovich indenter), h_{max} is the maximum penetration depth, and S is the contact stiffness estimated from the initial slope of the unloading curve at the P_{max}.

The indentation elastic modulus (E_{IT}) of the glass sample can be estimated as,

$$E_{IT} = (1 - \nu^2)\left[\frac{1}{E_r} - \frac{1-\nu_i^2}{E_i}\right]^{-1} \quad (4)$$

where E_i, ν_i represent the elastic modulus (1140 GPa) and Poisson ratio (0.07) of the diamond indenter probe used for indentation, respectively. E_r is the reduced elastic modulus,

$$E_r = \frac{S}{2}\sqrt{\frac{\pi}{A_p}}. \quad (5)$$

2.4 Indentation deformation analysis

To understand the nanomechanical response of the borosilicate glass series as a function of the composition, at least 10 crack-free indents were made using a Vickers indenter at a normal load of 100 mN with a dwell time of 15 s, employing a manual microhardness tester

(HMV-2, Shimadzu, Japan). A load of 100 mN was selected for making Vickers imprints that are large enough to be clearly discernable, yet a small enough load to ensure no radial/median cracks [14,53]. Also, previous theoretical and experimental analysis suggests that the strains under Vickers and Berkovich indenter tips are comparable [54]. Hence, the Vickers impression used in the indentation deformation analysis was corelated to the nanoindentation data obtained through Berkovich tip. Imaging of the residual Vickers imprints was carried out using an integrated AFM module (Nanite, Nanosurf, Switzerland). AFM imaging was executed over the indents at an imaging load of 20 nN in contact mode. Silicon cantilever tip with aluminum reflex coating having a nominal tip radius of 20 nm was used for imaging. The sharpness of the cantilever tip was also verified while switching between two glass compositions using a standard tip check sample (Budgetsensors, Bulgaria). Scanned AFM impressions were analyzed using a commercial software package (Scanning Probe Image Processing, Hørsholm, Denmark) for image processing. Figure 1(a) shows the processed image.

2.4.1 Densification estimation

To determine the indentation deformation mechanism as a function of composition, the protocol established by Yoshida et al. [37] was applied. This protocol helps in quantifying the densified volume upon annealing of the residual indents below the glass transition temperature (T_g), where only the recovery of the densified volume takes place and no structural relaxation [39]. Hence, the borosilicate glasses were annealed at $0.9T_g$ for 2 hours at ambient atmosphere. For every glass composition, topographic images of the indents were captured and analyzed before and after annealing. Figures 1 (c) and (d) shows the comparison of the 2D surface topographic images before and after annealing. Similarly, Figs. 1 (e) and (f)

reveals the comparison of the surface 3D topographic images before and after annealing, respectively.

For volume estimation, indent data before and after annealing was processed using Gwyddion software package. All the surface corrections and modifications which include flattening of the surface, averaged levelling of data points by fitting a plane was accomplished by the aforesaid software package. Further, the imported data from the software package was analyzed in a custom written programming code in MATLAB, which enabled the estimation of volumes below and above the surface. Figures 1(a) and (b) show a 2D glimpse of the volume estimation before and after annealing by the consideration of the volume above and below the surface. The densified volume can then be determined as [37].

$$V_R = \frac{(V_i^- - V_a^-) + (V_a^+ - V_i^+)}{V_i^-} \quad (6)$$

where V_R is the recovered volume, and V_i^- and V_i^+ represent the volume estimated below and above the surface, respectively, before annealing. Similarly, V_a^- and V_a^+ represent the volume below and above the surface, respectively, after annealing.

2.4.2 Shear flow estimation

To also estimate the shear flow or permanent plastic flow around the impression, the protocol proposed by Sellappan et al. [55] was followed, which also relies on AFM imaging of annealed indentation profiles. The volume of pile-up or shear flow above the surface can be estimated as,

$$V_P = \frac{(2V_i^+ - V_a^+)}{V_i^-} \quad (7)$$

where V_P indicates the volume pile-up ratio, for which volume of the pile-up above the surface before and after annealing are normalized by the densified volume before annealing as in Eq. 6.

3. Results and discussion

3.1 Nanoindentation of borosilicate glasses

3.1.1 Analysis of load-displacement curve

First, we focus on the elastoplastic behavior of the glasses obtained through depth sensing instrumented nanoindentation technique [56]. Figure 2 shows the load-displacement (*P-h*) curves obtained from the elastoplastic response of the borosilicate glasses used in this study. From the *P-h* plot, we observe that the curves corresponding to 37B-37Si, 24B-50Si, and 12B-62Si glasses nearly coincide with each other, showing a lower maximum penetration depth (h_{max}) in comparison to the other compositions. Similarly, the curves of 50B-24Si and 6B-68Si glasses coincide with each other with an intermediate h_{max} value. Finally, the 62B-12Si glass exhibits the maximum h_{max}. This implies that the hardness of the 62B-12Si should be low due to its lower resistance to penetration as confirmed by the h_{max} [1]. Accordingly, the hardness of 37B-37Si, 24B-50Si, and 12B-62Si must be higher, due to their lower penetration depth, followed by 50B-24Si and 6B-68Si. However, elastic behavior of glasses can also play a role in governing the hardness values [30,31,33]. Hence, it is necessary to understand the elasto-plastic behavior in detail.

3.1.2 Elasto-plastic analysis

Table S1 shows the hardness values of the alkali-alkaline borosilicate glass specimens used in this study. The hardness values are computed based on the contact area estimated from the initial slope of the unloading portion from the respective *P-h* curves as proposed by Oliver-Pharr[28]. Note that the tip roundness effect was ignored in the calculation of these hardness values. The results presented confirm that the calculated hardness values are as expected based on the *P-h* curves discussed earlier.

One of the major advantages of using nanoindentation technique in comparison to microindentation is that the elasticity values can be obtained from *P-h* curves along with the hardness [30–33,44,57]. To investigate the elasto-plastic behavior, we quantify the h_f/h_{max} ratio, which assesses the elastic behavior while retracting the indenter [57]. If no elastic recovery takes place, then the material is perfectly plastic with the h_f/h_{max} ratio equal to unity [30,57]. Based on this ratio, the elastic recovery index, $(h_{max}-h_f)/h_{max}$ or $1-h_f/h_{max}$, can be defined as a parameter that measures the relative elastic recovery upon unloading [31]. In this case, a perfectly plastic material gives elastic recovery index of 0 and vice versa. Likewise, the elastic deformation index $(h_{max}-h_c)/h_{max}$ or $1-h_c/h_{max}$ measures the relative elastic deformation surrounding the indented region [31].

Studies in the past have indicated that parameters such as elastic recovery index and elastic deformation index can be used for understanding the composition-dependent hardness and plastic behavior of glasses [30,31,33,44]. Hence, we here compute the elastic recovery index and elastic deformation index for the present glasses and relate these to the respective hardness values as shown in Figs. 3 (a) and (b). However, in the glass series used in our study, we observe that all the borosilicate glass specimens exhibit almost similar elastic recovery and deformation index. In other words, no composition-dependent trends in terms of the elastic

deformation or recovery behavior are observed (refer Fig. S1), although the glasses feature different hardness and elastic moduli (refer supplementary material Fig. S3). We observe that hardness and the indentation modulus exhibit a similar trend with composition. In general, hardness is governed by the network connectivity in glasses. However, elastic modulus is governed by the energy density. When the hardness of glass is mainly governed by densification—that is, the deformation of the network—then the elastic modulus can exhibit a trend similar to hardness.

The maximum penetration depth (h_{max}) has also been reported to be one of the critical parameters obtained from the load-displacement curves [57]. Hence, to understand the composition dependence, we plot h_{max} against the $[SiO_2]/([SiO_2] + [B_2O_3])$ molar ratio [1,20]. Intriguingly, three distinct hardness regimes are observed as discussed previously. That is, the glasses [(37B-37Si), (50Si-24B), (62Si-12B)] that exhibit higher hardness values appear to have maximum resistance to deformation, and hence the lower penetration depth as shown in Fig.S2. In other words, h_{max} decreases with increasing SiO_2 content until it reaches a minima at $[SiO_2]/([SiO_2] + [B_2O_3] \sim 0.5$, after which it increases with increasing SiO_2 content. This clearly reveals the role of composition in governing the elasto-plastic behavior upon indentation. The role of composition in governing the hardness is discussed in detail in the next section.

3.2 Effect of composition on microhardness and nanohardness

3.2.1 Microhardness and nanohardness

Figure 4 shows the nano and microhardness values for the glass compositions considered in the present study. The comparison shows that the hardness values obtained from nanoindentation and microindentation are different. As hardness is not an intrinsic material

property, the variation can be explained based on differences in the tip geometry, tip bluntness, and the load applied [58,59]. In our present experiment, we have used 50 mN load whereas in the compared microindentation data, 250 mN[1] load was used. Variation could also be possible due to the difference in tip geometry, i.e., Berkovich tip used in this nanoindentation experiment versus Vickers tip used in the compared microindentation data [1]. Three-sided Berkovich indenter has a relatively sharper tip than the four-sided Vickers indenter [60]. Even though our nanoindentation observation statistically follows the similar trend as the previously published result on the same compositions, the relatively higher sharpness/pointedness of the Berkovich indenter tip [61] might also be a reason for such pronounced boron anomaly transition at ratio = 0.7.

3.2.2 Role of *R* and *K* ratios on hardness

To investigate the role of composition on the hardness, we analyze the variation of hardness with the *K* ratio defined as $K = [SiO_2]/([SiO_2] + [B_2O_3])$ [1,14,20,21,44,62] and the *R* ratio defined as $R = ([Na_2O] + [CaO])/[B_2O_3]$ [1,14,20,21,44] as shown in Figs. 4 and 5, respectively. These ratios have been widely adopted in the glass literature to understand the governing role of structural species in the borosilicate glass compositions. As shown in Fig. 4 (triangle legend), we observe that hardness exhibits a non-monotonic response with *K*, that is, increasing from a minimum value of 7.62 GPa to attain a maximum value of 9.27 GPa before decreasing further to 8.50 GPa. Specifically, the hardness value increases until the *K* ratio equals 0.7 (see Fig. 4), which can be considered as boron anomaly boundary, and thereafter, a dip in the hardness values is observed. Previous research has indicated that the transition from B^3 to B^4 increases monotonically with the *K* ratio [1,17], suggesting that the decrease in hardness values with *K*-ratios above 0.7 can be attributed to the depolymerization of the silicate network.

Further, to understand the role of network modifiers (CaO, Na_2O) on boron network, hardness values are plotted against the *R* ratio (Figure 5). Figure 5 reveals a pronounced boron anomaly boundary at *R* ratio of 1, beyond which the hardness tends to decrease. This can be understood by the fact that, at composition with higher concentration of B_2O_3 (62B-12Si with *R* ratio of 0.4), the shortage of Na and Ca cations for charge compensation of B^3 units makes the structure more open (and less polymerized) due to the presence of more trigonal planar structures. Such lower compactness results in a decreased resistance of the structure to plastic deformation, and hence lower hardness values. In addition, from thereon, the hardness values tend to increase with *R*-ratio until the boron anomaly line, that is, from boron-rich glass composition to relatively less boron concentration. Here, Na^+ and Ca^{2+} ions will be available for charge compensating the B^3 structural units to B^4 structural units. Therefore, an increase in hardness is observed due to such increased connectivity offered by the B^4 structural units. However, after crossing the boron anomaly boundary ($R > 1$), hardness reduces with excess availability of charge compensators like Na and Ca cations. The region beyond the boron anomaly line is rich in silica (lower boron concentration). Consequently, the excess charges are responsible in depolymerizing the silicate network, ultimately leading to a drop in hardness values.

3. 3 Indentation deformation mechanisms

For understanding the deformation mechanisms of the borosilicate glasses used in our study, we have employed Vickers indenter tip as reported in other studies [14,37,38,43,55,63], which had successfully demonstrated its use in the estimation of densification and shear flow contributions to the total indentation deformation.

3.3.1 Indentation pile-up estimation

During the process of indentation, the material beneath the indenter is heavily compressed due to the high pressure generated by the sharp contact loading [25], which leads to an increase in the local density of the material. Similarly, the material which manifests above the surface around the impression edges (as clearly shown in Figs. 1(d), (f)) are identified as pile-ups [36]. Note that these pile-ups are also a form of permanent deformation [31,64].

Earlier research has suggested that such pile-ups have a strong relation with the glass composition [43]. Hence, we attempted to quantify the normalized indentation pile-ups (V_i^+/V_i^-) before annealing. Table 2 presents the nominal mean diagonal length (d_i), indentation depth (h_i), volume below (V_i^-) and above (V_i^+), % indentation pile-up (V_i^+ / V_i^-) obtained from AFM images of the various borosilicate glasses indented using Vickers geometry before annealing. Figure 6 shows the estimated fractional indentation pile-up (V_i^+/V_i^-) as a function of *R*-ratio by considering the pile-up volume above the surface (V_i^+) and the densified volume below the surface (V_i^-). We observe that the indentation pile-up ratio does not exhibit any pronounced composition-dependent behavior, although it tends to decrease slightly with increasing *R*-ratio. However, the hardness of the glasses indeed exhibits a composition-dependent behavior as demonstrated earlier.

3.3.2 Estimation of volume recovery

It has been shown in various experimental observations that the impression cavity shrinks upon thermal annealing at $0.9T_g$ [14,37,38,65]. The recovered volume measured on a 3D profile upon annealing corresponds to the volume densified during indentation. Figure 7 reveals the quantified recovered volume ratio (V_R) for the borosilicate glass compositions as a function of *R*-ratio. Interestingly, in this plot, the composition-dependent behavior can be clearly

observed. Apart from the volume recovery, the diagonal recovery (d_a) after annealing (Table 3) also reveals the same trend as the volume recovery ratio. In addition, we can identify three distinct different regions in V_R. The recovery behavior of boron-rich composition for R values less than 0.5 (62B-12Si, 50B-24Si) are similar. Likewise, the recovery behavior for compositions with R values between 0.5 to 2, i.e., 37B-37Si, 24B-50Si, and 12B-62Si, falls in the same region. Finally, the recovery behavior of the silica-rich 6B-68Si composition (R value of 4) is different from the other two regions. This is because densification plays a major role in the indentation deformation of boron-rich compositions [14,44].

Indentation deformation studies on boron-rich glasses have revealed that the more open structure of borate network comprising a larger fraction of BO_3 units promotes densification [66]. Therefore, such larger volume recovery for boron-rich glass compositions can be attributed to the open structure of such glasses. It has also been found that under the high pressure generated during indentation process, local conversion of B^3 units into B^4 units occurs [44]. Even though the majority of such conversion relaxes back to B^3 units after unloading, a fraction of structural change is retained [14]. Hence, it can be argued that in the case of 62B-12Si, a fraction of retained B^4 structural units has resulted in reduced volume recovery due to a minor change in free volume. As a result, the volume recovery of 62B-12Si and 50B-24Si is almost similar. On the other hand, for intermediate R values, a minimum value of V_R can be noticed.

Recalling that the conversion from B^3 to B^4 units increases with R value, it has been noticed for higher values of R or with increasing concentration of Na_2O and CaO that the created B^4 units link to silicate networks [14]. Such connectivity between silicate and borate networks reduces the tendency of borosilicate networks to densify [14]. Hence, reduced V_R can be observed for R values between 0.5 to 2. Lastly, the relatively higher volume recovery for

glass with R value of 4 can be related to the higher concentration of silica [23]. As most of the network modifiers will be utilized in the conversion of available B^3 to B^4 units, the remaining modifiers will result in depolymerizing the silicate network[1]. Since the content of silica is slightly higher here, the deformation mode will be primarily controlled by densification.

3.3.3 Estimation of Volume Pile-up

Sellappan et al. [55] have extended the protocol proposed by Yoshida et al. [37] to estimate the plastic pile-up volume around the impression cavity to distinguish the effect of densification. Figure 8 shows the percentage volume pile-up measured using such protocol as a function of the R ratio. Although there is no prominent composition dependent behavior, we observe a slight decrease in the extent of pile-up with increasing R-ratio. Similarity can be drawn between the trend exhibited by the percentage indentation pile-up and the percentage volume pile-up, which might be because pile-up is a form of shear flow deformation [43], which cannot be recovered by thermal activation processes such as sub-T_g annealing [37].

3.3.4 Linking hardness and volume recovery

In previous work, the relation between packing density and hardness has been investigated[14,53] . Here, Fig. 9 shows a strong relationship between hardness and the volume recovery upon sub-T_g annealing of indented samples. Specifically, we observe that hardness exhibits a linear relationship with the inverse of the percentage volume recovery. Boron-rich glass compositions exhibit an open structure offered by trigonal planar B^3 units [1,66], which, in turn, makes them less rigid, allowing large deformation upon loading. This leads to an increased densified volume, lower hardness values, and higher volume recovery. The increased hardness for R values of 0.5 to 2 is due to the transition from B^3 to B^4, which has led to the drop in volume recovery [1,14]. This is because of the reduced free volume by such

transition [14,44]. Further, the hardness and densification for compositions with *R* values between 0.5 to 2 are found to be comparable. Finally, the decrease in hardness is due to depolymerization of the silicate network [1,17] where the volume recovery slightly increases due to the relatively higher availability of silicate networks for densifying. The overall mechanism governing this observation could be explained as follows. Glasses having an open structure exhibit decreased rigidity and increased densification upon indentation, which leads to a reduction in hardness and an increase in the volume recovery upon annealing. On the other hand, glasses with higher degree of polymerization exhibit increased rigidity and hence decreased densification upon indentation, which leads to decreased values of volume recovery and increased values of hardness. Thus, this inverse relationship between hardness and densified volume agrees with the observation that the glasses having increased network connectivity exhibit increased hardness.

4. Conclusion

We have analyzed the indentation deformation of an alkali-alkaline earth borosilicate glass series. Specifically, we have employed nanoindentation for understanding the glasses' elasto-plastic behavior followed by thermal annealing for the quantification of indentation-induced deformation mechanisms. The glasses exhibit a non-monotonic variation in hardness with composition in agreement with the boron anomaly. Based on the *R* and *K* ratios, we show that the trend in the hardness can be reconciled with the glasses having *R* ratio corresponding to 1, exhibiting maximum hardness. We observe that hardness exhibits a strong inverse relation with the indentation volume recovery in the compositions considered here, which is explained in terms of the network connectivity. The universality of this observation to other borosilicate glass compositions requires further experiments. In any case, the presence and

concentration of network modifying cations is found to play a key role in governing the indentation deformation mechanism of borosilicate glasses.

Acknowledgement

NMAK acknowledges the financial support for this research provided by the Department of Science and Technology, India, under the INSPIRE faculty scheme (DST/INSPIRE/04/2016/002774) and DST SERB Early Career Award (ECR/2018/002228). NNG would like to acknowledge the financial support from DST, SERB (CRG/2020/002062).

References

1. Smedskjaer MM, Mauro JC, Youngman RE, Hogue CL, Potuzak M, Yue Y. Topological Principles of Borosilicate Glass Chemistry. J Phys Chem B. 2011 Nov 10;115(44):12930–46.

2. Varshneya AK. Fundamentals of Inorganic Glasses. Elsevier; 2013. 591 p.

3. Shelby JE. Introduction to Glass Science and Technology [Internet]. 2005 [cited 2019 Jul 2]. Available from: https://pubs.rsc.org/en/content/ebook/978-0-85404-639-3

4. Fu Q, Rahaman MN, Fu H, Liu X. Silicate, borosilicate, and borate bioactive glass scaffolds with controllable degradation rate for bone tissue engineering applications. I. Preparation and in vitro degradation. Journal of Biomedical Materials Research Part A. 2010 Oct 1;95A(1):164–71.

5. Guan M, Zhang XY, Yang KJ, Wang TT, Liu FF, Sun ML, et al. Difference in radiation effects of sodium borosilicate glass and vitreous silica with ions. Journal of Non-Crystalline Solids. 2019 Aug 15;518:118–22.

6. Peng HB, Sun ML, Yang KJ, Chen H, Yang D, Yuan W, et al. Effect of irradiation on hardness of borosilicate glass. Journal of Non-Crystalline Solids. 2016 Jul 1;443:143–7.

7. Plodinec MJ. Borosilicate glasses for nuclear waste imobilisation. Glass Technology. 2000 Dec 1;41(6):186–92.

8. Ojovan MI, Lee WE. Glassy Wasteforms for Nuclear Waste Immobilization. Metall Mater Trans A. 2011 Apr 1;42(4):837–51.

9. Ellison A, Cornejo IA. Glass Substrates for Liquid Crystal Displays. International Journal of Applied Glass Science. 2010;1(1):87–103.

10. Peng S, Ke Z, Cao X, Shan C, Zhao F, Guan M, et al. A novel type of borosilicate glass with excellent chemical stability and high ultraviolet transmission. Journal of Non-Crystalline Solids. 2020 Jan 15;528:119735.

11. Wondraczek L, Bouchbinder E, Ehrlicher A, Mauro JC, Sajzew R, Smedskjaer MM. Advancing the Mechanical Performance of Glasses: Perspectives and Challenges. Advanced Materials. n/a(n/a):2109029.

12. Yiannopoulos YD, Chryssikos GD, Kamitsos EI. Structure and properties of alkaline earth borate glasses. Physics and Chemistry of Glasses. 2001 Jun 1;42(3):164–72.

13. Jaccani SP, Huang L. Understanding Sodium Borate Glasses and Melts from Their Elastic Response to Temperature. International Journal of Applied Glass Science. 2016 Dec 1;7(4):452–63.

14. Limbach R, Winterstein-Beckmann A, Dellith J, Möncke D, Wondraczek L. Plasticity, crack initiation and defect resistance in alkali-borosilicate glasses: From normal to anomalous behavior. Journal of Non-Crystalline Solids. 2015 Jun 1;417–418:15–27.

15. Yoshida S, Tanaka H, Hayashi T, Matsuoka J, Soga N. Scratch Resistance of Sodium Borosilicate Glass. Journal of the Ceramic Society of Japan. 2001;109(1270):511–5.

16. Malchow P, Johanns KE, Möncke D, Korte-Kerzel S, Wondraczek L, Durst K. Composition and cooling-rate dependence of plastic deformation, densification, and cracking in sodium borosilicate glasses during pyramidal indentation. Journal of Non-Crystalline Solids. 2015 Jul 1;419:97–109.

17. Wang M, Anoop Krishnan NM, Wang B, Smedskjaer MM, Mauro JC, Bauchy M. A new transferable interatomic potential for molecular dynamics simulations of borosilicate glasses. Journal of Non-Crystalline Solids. 2018 Oct 15;498:294–304.

18. Kieu LH, Delaye JM, Cormier L, Stolz C. Development of empirical potentials for sodium borosilicate glass systems. Journal of Non-Crystalline Solids. 2011 Sep 15;357(18):3313–21.

19. Tuheen MI, Deng L, Du J. A comparative study of the effectiveness of empirical potentials for molecular dynamics simulations of borosilicate glasses. Journal of Non-Crystalline Solids. 2021 Feb 1;553:120413.

20. Yun YH, Bray PJ. Nuclear magnetic resonance studies of the glasses in the system Na2O□B2O3□SiO2. Journal of Non-Crystalline Solids. 1978 Mar 1;27(3):363–80.

21. Zhao Y, Zhang X, Yuan W, Liu F, Sun M, Peng H, et al. Composition effects on mechanical properties of pristine sodium borosilicate glass. International Journal of Applied Glass Science. 2019;10(3):363–70.

22. Barlet M, Kerrache A, Delaye JM, Rountree CL. SiO2–Na2O–B2O3 density: A comparison of experiments, simulations, and theory. Journal of Non-Crystalline Solids. 2013 Dec 15;382:32–44.

23. Januchta K, Smedskjaer MM. Indentation deformation in oxide glasses: Quantification, structural changes, and relation to cracking. Journal of Non-Crystalline Solids: X. 2019 Mar;1:100007.

24. Kasimuthumaniyan S, Gosvami NN, Krishnan NMA. Towards understanding the scratchability in functional glasses. Ceramics International. 2021 Aug 1;47(15):20821–43.

25. Rouxel T. Driving force for indentation cracking in glass: composition, pressure and temperature dependence. Philosophical Transactions of the Royal Society A: Mathematical, Physical and Engineering Sciences. 2015 Mar 28;373(2038):20140140–20140140.

26. Rouxel T, Jang J il, Ramamurty U. Indentation of glasses. Progress in Materials Science. 2021 Aug 1;121:100834.

27. Lawn B. Fracture of Brittle Solids [Internet]. 2nd ed. Cambridge: Cambridge University Press; 1993 [cited 2020 Aug 24]. (Cambridge Solid State Science Series). Available from: https://www.cambridge.org/core/books/fracture-of-brittle-solids/B1EC1413BDBA1DCF49E1665D4B0A20F3

28. Oliver WC, Pharr GM. An improved technique for determining hardness and elastic modulus using load and displacement sensing indentation experiments. Journal of Materials Research. 1992 Jun 1;7(6):1564–83.

29. Yoshida S. Indentation deformation and cracking in oxide glass –toward understanding of crack nucleation. Journal of Non-Crystalline Solids: X. 2019 Mar 1;1:100009.

30. Dey A, Mukhopadhyay AK. Nanoindentation of Brittle Solids. CRC Press; 2014. 480 p.

31. Kasimuthumaniyan S, Reddy AA, Krishnan NMA, Gosvami NN. Understanding the role of post-indentation recovery on the hardness of glasses: Case of silica, borate, and borosilicate glasses. Journal of Non-Crystalline Solids. 2020 Apr 15;534:119955.

32. Li X, Jiang L, Li J, Mohagheghian I, Dear JP, Li L, et al. Elastic-plastic deformation in ion-exchanged aluminosilicate glass by loading rate dependent nanoindentation. Journal of Non-Crystalline Solids. 2018 Jul 1;491:79–88.

33. Miura T, Benino Y, Sato R, Komatsu T. Universal hardness and elastic recovery in Vickers nanoindentation of copper phosphate and silicate glasses. Journal of the European Ceramic Society. 2003 Mar 1;23(3):409–16.

34. Yoshida S, Kato M, Yokota A, Sasaki S, Yamada A, Matsuoka J, et al. Direct observation of indentation deformation and cracking of silicate glasses. Journal of Materials Research. 2015 Aug 1;30(15):2291–9.

35. Rouxel T, Ji H, Hammouda T, Moréac A. Poisson's Ratio and the Densification of Glass under High Pressure. Phys Rev Lett. 2008 Jun 3;100(22):225501.

36. Rouxel T, Ji H, Guin JP, Augereau F, Rufflé B. Indentation deformation mechanism in glass: Densification versus shear flow. Journal of Applied Physics. 2010 May;107(9):094903.

37. Yoshida S, Sanglebœuf JC, Rouxel T. Quantitative evaluation of indentation-induced densification in glass. J Mater Res. 2005 Dec 1;20(12):3404–12.

38. Januchta K, Youngman RE, Goel A, Bauchy M, Rzoska SJ, Bockowski M, et al. Structural origin of high crack resistance in sodium aluminoborate glasses. Journal of Non-Crystalline Solids. 2017 Mar 15;460:54–65.

39. Aakermann KG, Januchta K, Pedersen JAL, Svenson MN, Rzoska SJ, Bockowski M, et al. Indentation deformation mechanism of isostatically compressed mixed alkali aluminosilicate glasses. Journal of Non-Crystalline Solids. 2015 Oct 15;426:175–83.

40. Kazembeyki M, Bauchy M, Hoover CG. New insights into the indentation size effect in silicate glasses. Journal of Non-Crystalline Solids. 2019 Oct 1;521:119494.

41. He H, Hahn SH, Yu J, Qiao Q, van Duin ACT, Kim SH. Friction-induced subsurface densification of glass at contact stress far below indentation damage threshold. Acta Materialia. 2020 May 1;189:166–73.

42. Wang W, Li Z, Yao P, Li J, Chen F, Liu Y. Sink-in/pile-up formation and crack nucleation mechanisms of high purity fused silica and soda-lime silica glass during nanoindentation experiments. Ceramics International. 2020 Oct 15;46(15):24698–709.

43. Barlet M, Delaye JM, Charpentier T, Gennisson M, Bonamy D, Rouxel T, et al. Hardness and toughness of sodium borosilicate glasses via Vickers's indentations. Journal of Non-Crystalline Solids. 2015 Jun;417–418:66–79.

44. Malchow P, Johanns KE, Möncke D, Korte-Kerzel S, Wondraczek L, Durst K. Composition and cooling-rate dependence of plastic deformation, densification, and cracking in sodium borosilicate glasses during pyramidal indentation. Journal of Non-Crystalline Solids. 2015 Jul 1;419:97–109.

45. Kumar R, Jan A, Bauchy M, Krishnan NMA. Effect of irradiation on the atomic structure of borosilicate glasses. Journal of the American Ceramic Society. 2021;104(12):6194–206.

46. Gin S, Beaudoux X, Angéli F, Jégou C, Godon N. Effect of composition on the short-term and long-term dissolution rates of ten borosilicate glasses of increasing complexity from 3 to 30 oxides. Journal of Non-Crystalline Solids. 2012 Sep 15;358(18):2559–70.

47. Tadjiev DR, Hand RJ. Surface hydration and nanoindentation of silicate glasses. Journal of Non-Crystalline Solids. 2010 Jan 15;356(2):102–8.

48. Kilinc E, Hand RJ. Mechanical properties of soda–lime–silica glasses with varying alkaline earth contents. Journal of Non-Crystalline Solids. 2015 Dec 1;429:190–7.

49. Hand RJ, Tadjiev DR. Mechanical properties of silicate glasses as a function of composition. Journal of Non-Crystalline Solids. 2010 Oct 1;356(44):2417–23.

50. de Macedo GNBM, Sawamura S, Wondraczek L. Lateral hardness and the scratch resistance of glasses in the Na2O-CaO-SiO2 system. Journal of Non-Crystalline Solids. 2018 Jul 15;492:94–101.

51. Liu H, Smedskjaer MM, Tao H, Jensen LR, Zhao X, Yue Y. A medium range order structural connection to the configurational heat capacity of borate–silicate mixed glasses. Phys Chem Chem Phys. 2016 Apr 20;18(16):10887–95.

52. Hackett BL, Wereszczak AA, Pharr GM. Effect of aqueous-based mechanical polishing on the nanoindentation response of borosilicate glasses. International Journal of Applied Glass Science. 2019;10(3):302–6.

53. Yoshida S, Nishikubo Y, Konno A, Sugawara T, Miura Y, Matsuoka J. Fracture- and Indentation-Induced Structural Changes of Sodium Borosilicate Glasses. International Journal of Applied Glass Science. 2012;3(1):3–13.

54. Larsson PL, Giannakopoulos AE, SÖderlund E, Rowcliffe DJ, Vestergaard R. Analysis of Berkovich indentation. International Journal of Solids and Structures. 1996 Jan 1;33(2):221–48.

55. Sellappan P, Rouxel T, Celarie F, Becker E, Houizot P, Conradt R. Composition dependence of indentation deformation and indentation cracking in glass. Acta Materialia. 2013 Sep 1;61(16):5949–65.

56. Fischer-Cripps AC. Nanoindentation Testing. In: Fischer-Cripps AC, editor. Nanoindentation [Internet]. New York, NY: Springer New York; 2011 [cited 2019 May 24]. p. 21–37. (Mechanical Engineering Series). Available from: https://doi.org/10.1007/978-1-4419-9872-9_2

57. Oliver WC, Pharr GM. Measurement of hardness and elastic modulus by instrumented indentation: Advances in understanding and refinements to methodology. J Mater Res. 2004 Jan;19(1):3–20.

58. Swadener JG, George EP, Pharr GM. The correlation of the indentation size effect measured with indenters of various shapes. Journal of the Mechanics and Physics of Solids. 2002 Apr 1;50(4):681–94.

59. Sakharova NA, Fernandes JV, Antunes JM, Oliveira MC. Comparison between Berkovich, Vickers and conical indentation tests: A three-dimensional numerical simulation study. International Journal of Solids and Structures. 2009 Mar 1;46(5):1095–104.

60. Dukino RD, Swain MV. Comparative Measurement of Indentation Fracture Toughness with Berkovich and Vickers Indenters. Journal of the American Ceramic Society. 1992 Dec 1;75(12):3299–304.

61. Chudoba T, Schwaller P, Rabe R, Breguet JM, Michler J. Comparison of nanoindentation results obtained with Berkovich and cube-corner indenters. Philosophical Magazine. 2006 Nov 21;86(33–35):5265–83.

62. Kumar R, Jan A, Bauchy M, Krishnan NMA. Effect of irradiation on the atomic structure of borosilicate glasses. Journal of the American Ceramic Society [Internet]. [cited 2021 Aug 17];n/a(n/a). Available from: https://ceramics.onlinelibrary.wiley.com/doi/abs/10.1111/jace.18013

63. Qiao A, To T, Stepniewska M, Tao H, Calvez L, Zhang X, et al. Deformation mechanism of a metal–organic framework glass under indentation. Physical Chemistry Chemical Physics. 2021;23(31):16923–31.

64. Zhou X, Jiang Z, Wang H, Yu R. Investigation on methods for dealing with pile-up errors in evaluating the mechanical properties of thin metal films at sub-micron scale on hard substrates by nanoindentation technique. Materials Science and Engineering: A. 2008 Aug;488(1–2):318–32.

65. Neely JE, Mackenzie JD. Hardness and low-temperature deformation of silica glass. J Mater Sci. 1968 Nov 1;3(6):603–9.

66. Kato Y, Yamazaki H, Kubo Y, Yoshida S, Matsuoka J, Akai T. Effect of B_2O_3 content on crack initiation under Vickers indentation test. Journal of the Ceramic Society of Japan. 2010;118(1381):792–8.

CAPTION LIST

Table 1: Experimental glass composition in mol % and other properties [1].

Table 2: Experimental values of nominal mean diagonal length (d_i), indentation depth (h_i), volume below (V_i^-) and above (V_i^+), % indentation pile-up (V_i^+ / V_i^-) obtained from AFM images of the various borosilicate glasses indented using Vickers geometry before annealing.

Table 3: Experimental values of nominal mean diagonal length (d_a), indentation depth (h_a), volume below (V_a^-) and above (V_a^+), % volume recovery (V_r), % volume pile-up (V_p) obtained from AFM images of the various borosilicate glasses indented using Vickers geometry after annealing.

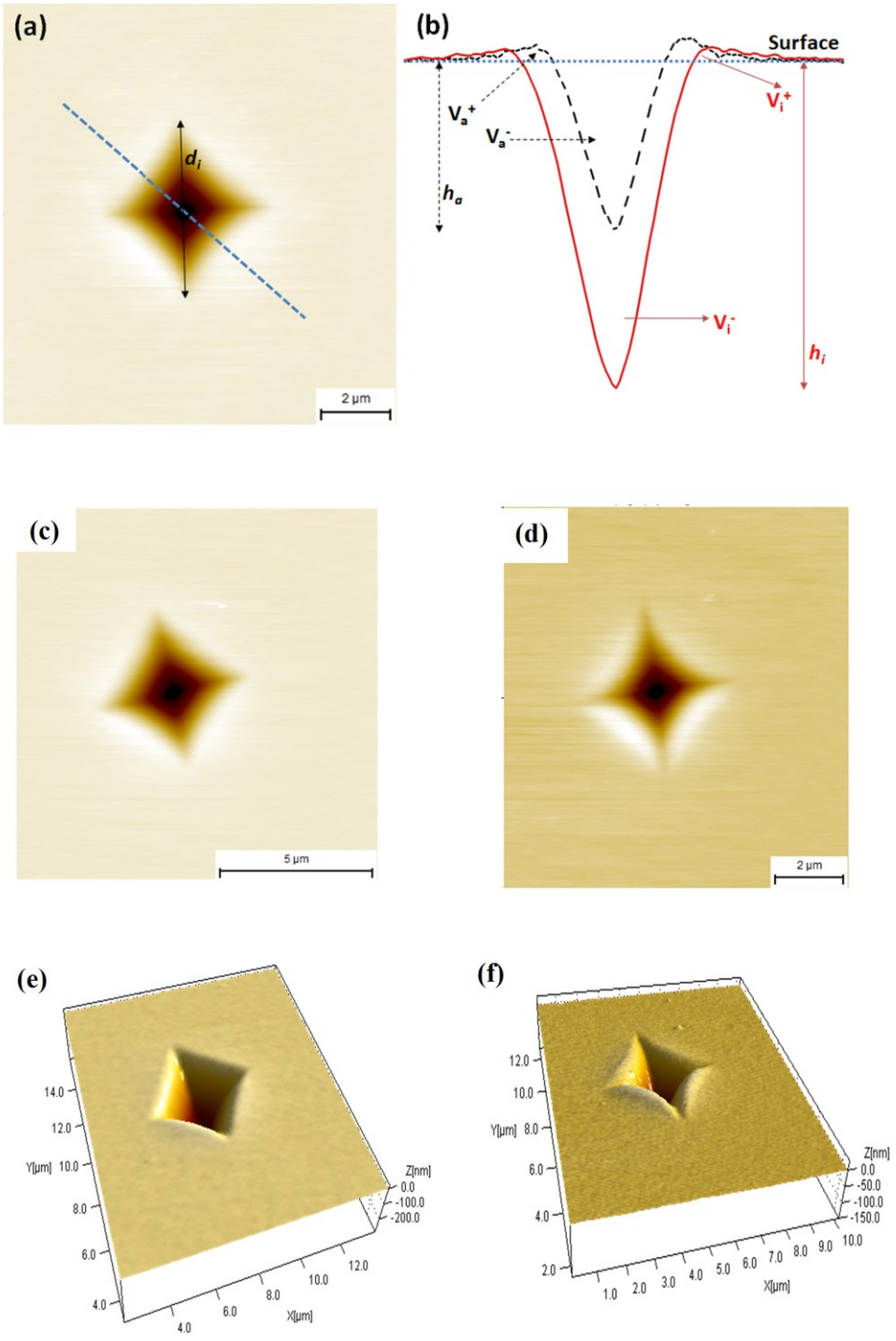

Figure 1. (a) Typical AFM image of a residual Vickers impression (dotted line is drawn to reveal the corresponding depth profile for the impression), **(b)** Depth profile revealing the evolution of the impression before (red solid line) and after (black dotted line) annealing. V_i^+, V_i^- indicates the volume above and below the surface (blue dotted line) before annealing.

Similarly, V_a^+, V_a^- represents the volume above and below the surface after annealing. h_i and h_a stands for depth below the surface before and after annealing, respectively. The depth profile corresponds to the 62B-12Si borosilicate glass specimen. **(c), (e)** Represents the typical 2D and 3D view of a residual Vickers impression before annealing, respectively. **(d), (f)** Represents the typical 2D and 3D view of residual Vickers impression after annealing, respectively.

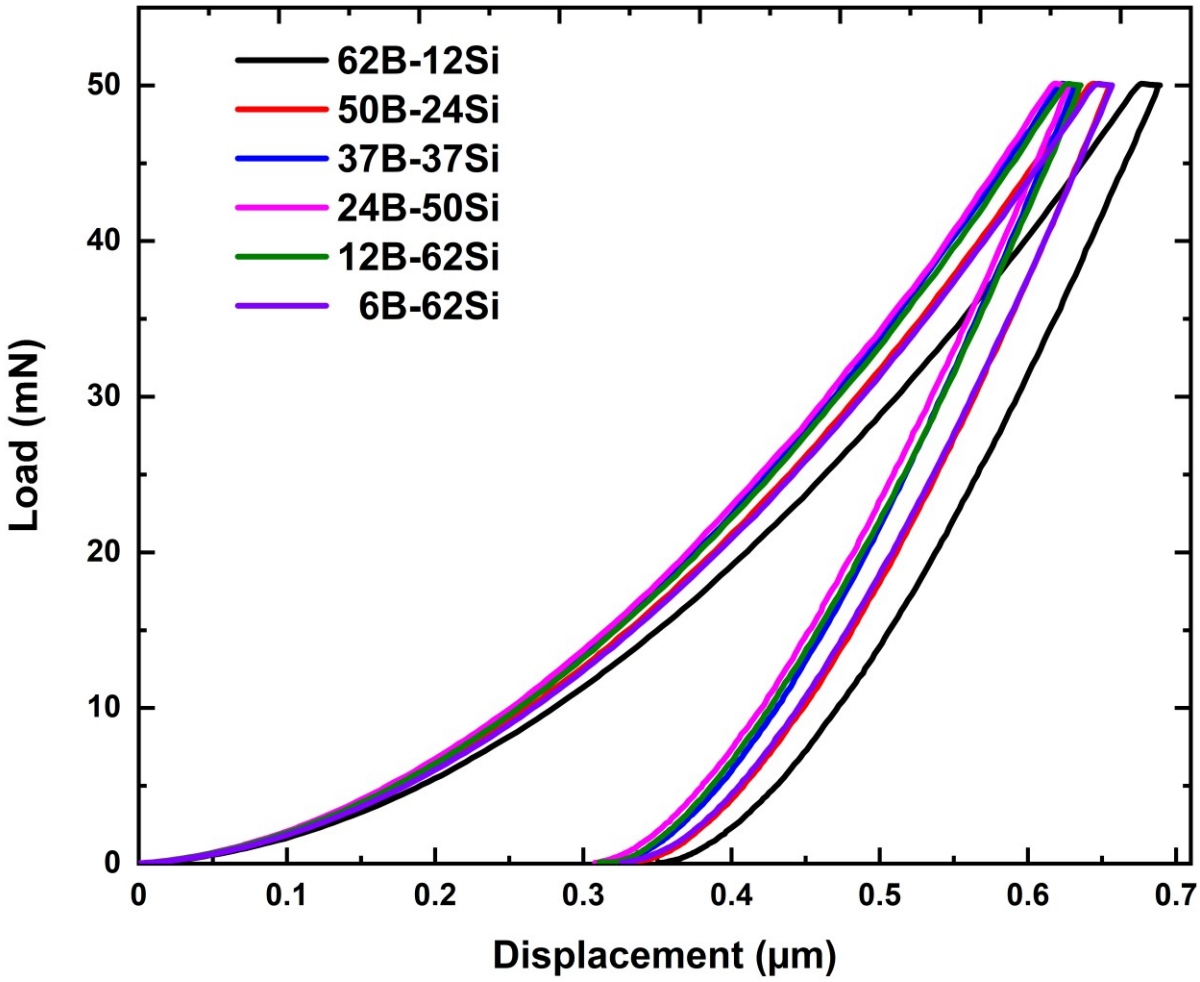

Figure 2. Load displacement curves of borosilicate glass samples of different compositions

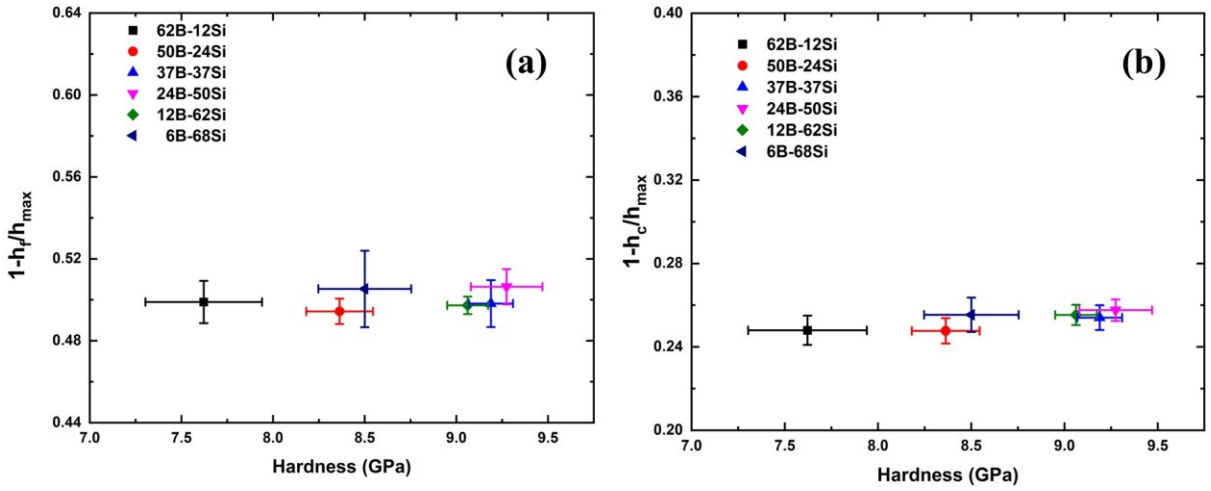

Figure 3 (a) *1-h_f/ h_{max}* ratio showing the elastic recovery obtained from nanoindentation tests for different borosilicate glass samples.

(b) *1-h_c /h_{max}* ratio obtained from nanoindentation showing the elastic deformation of different borosilicate glasses and their dependence on the hardness

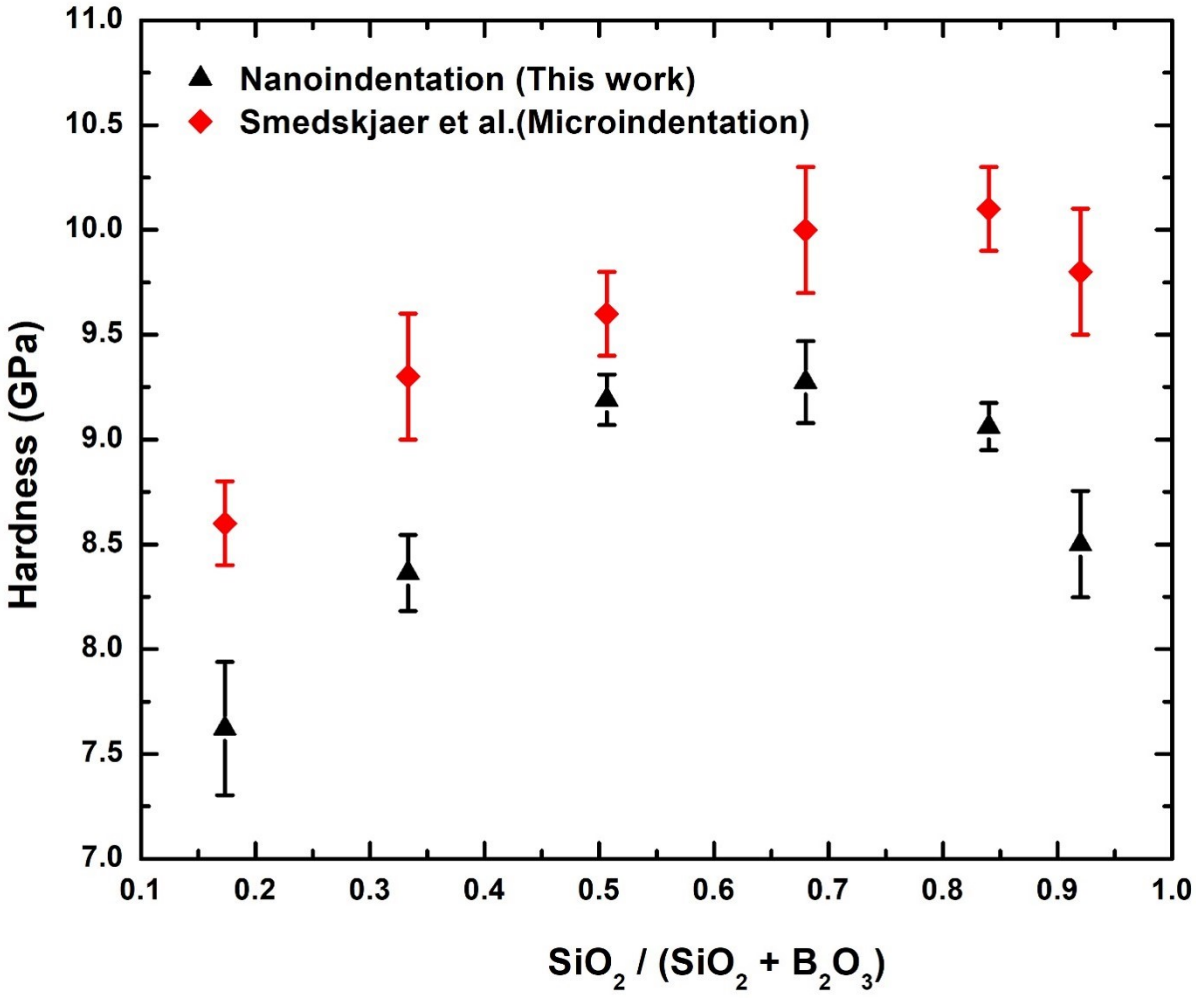

Figure 4. Relation between the hardness and $[SiO_2]/([SiO_2] + [B_2O_3])$ molar ratio (*K* value). Comparisons are drawn between nanohardness and microhardness[1].

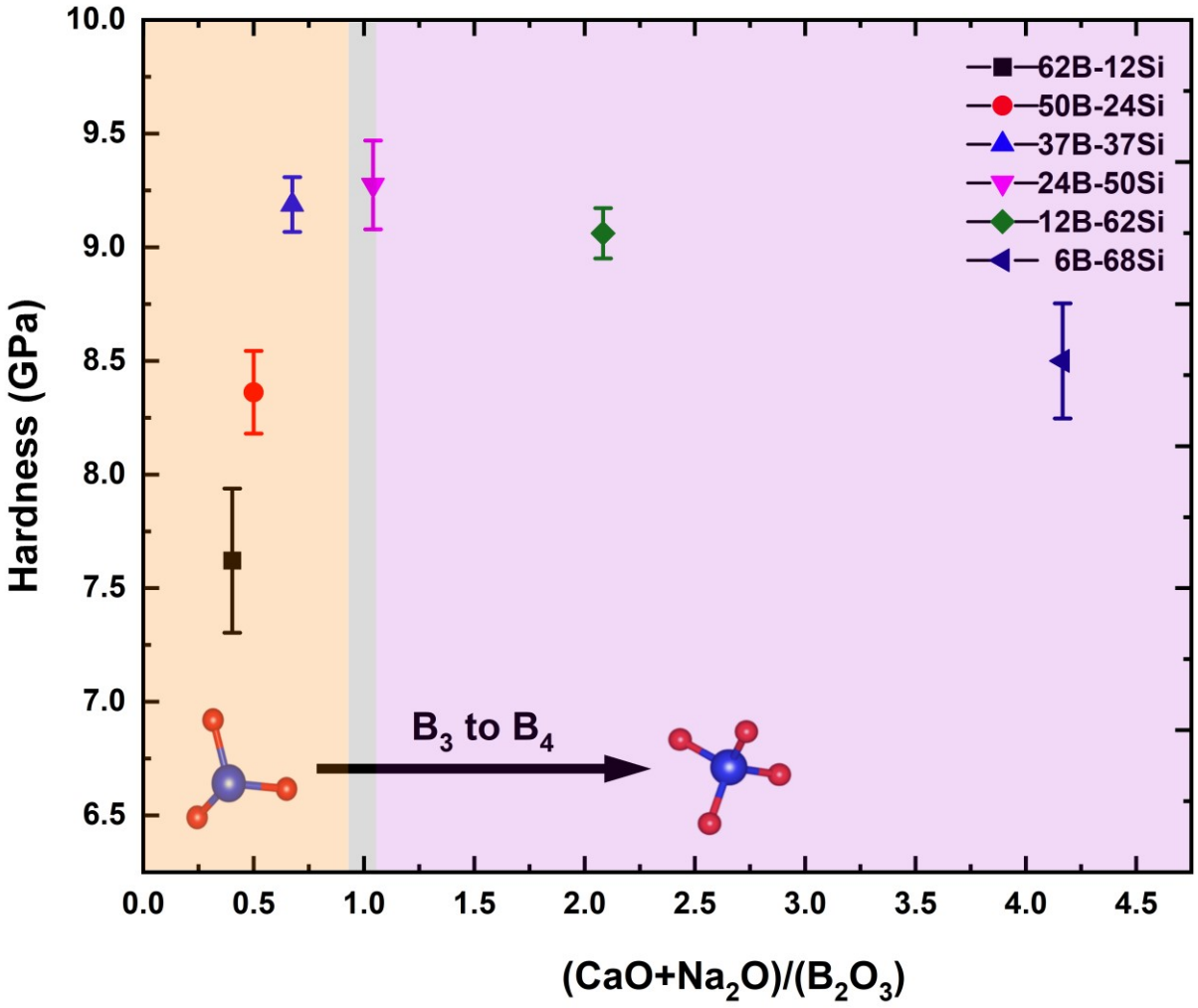

Figure 5. Relation between hardness and network modifiers to boron molar ratio (*R* value).

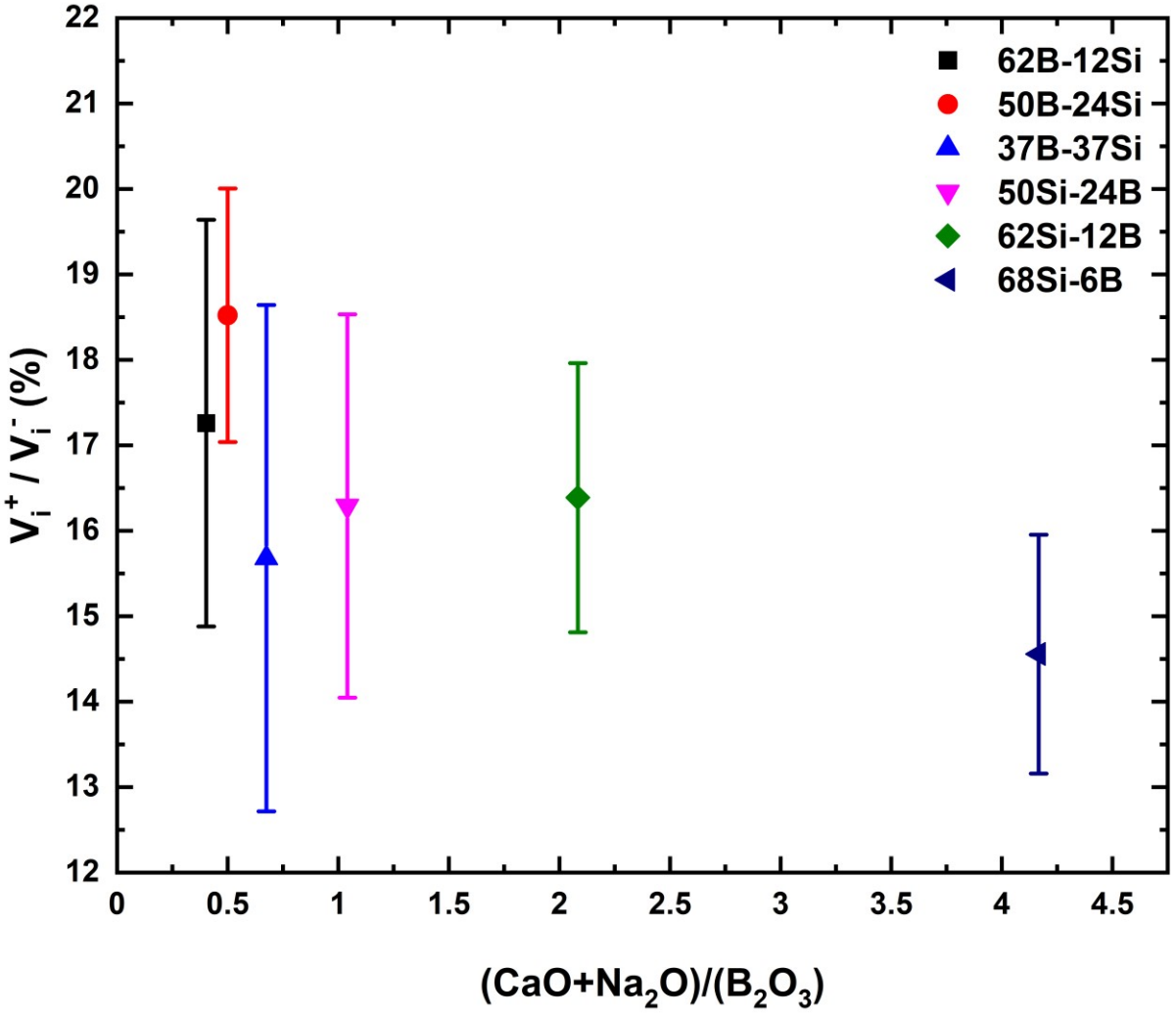

Figure 6. Relation between the indentation pileup before annealing and the network modifiers to boron molar ratio (*R* value).

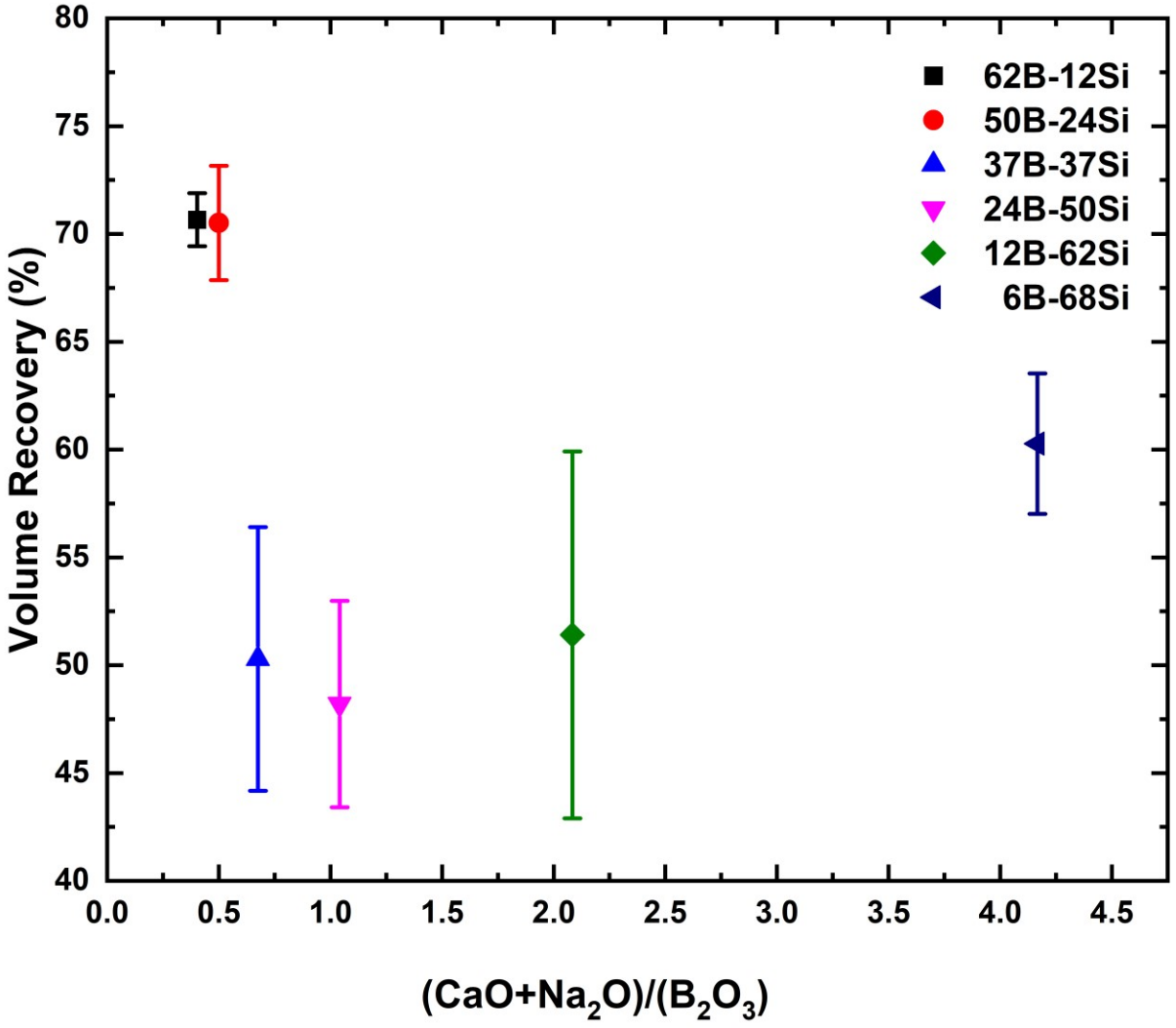

Figure 7. Relation between the fractional volume recovery (V_R) estimated by following Yoshida et al. [37] protocol and the network modifiers to boron molar ratio (R value).

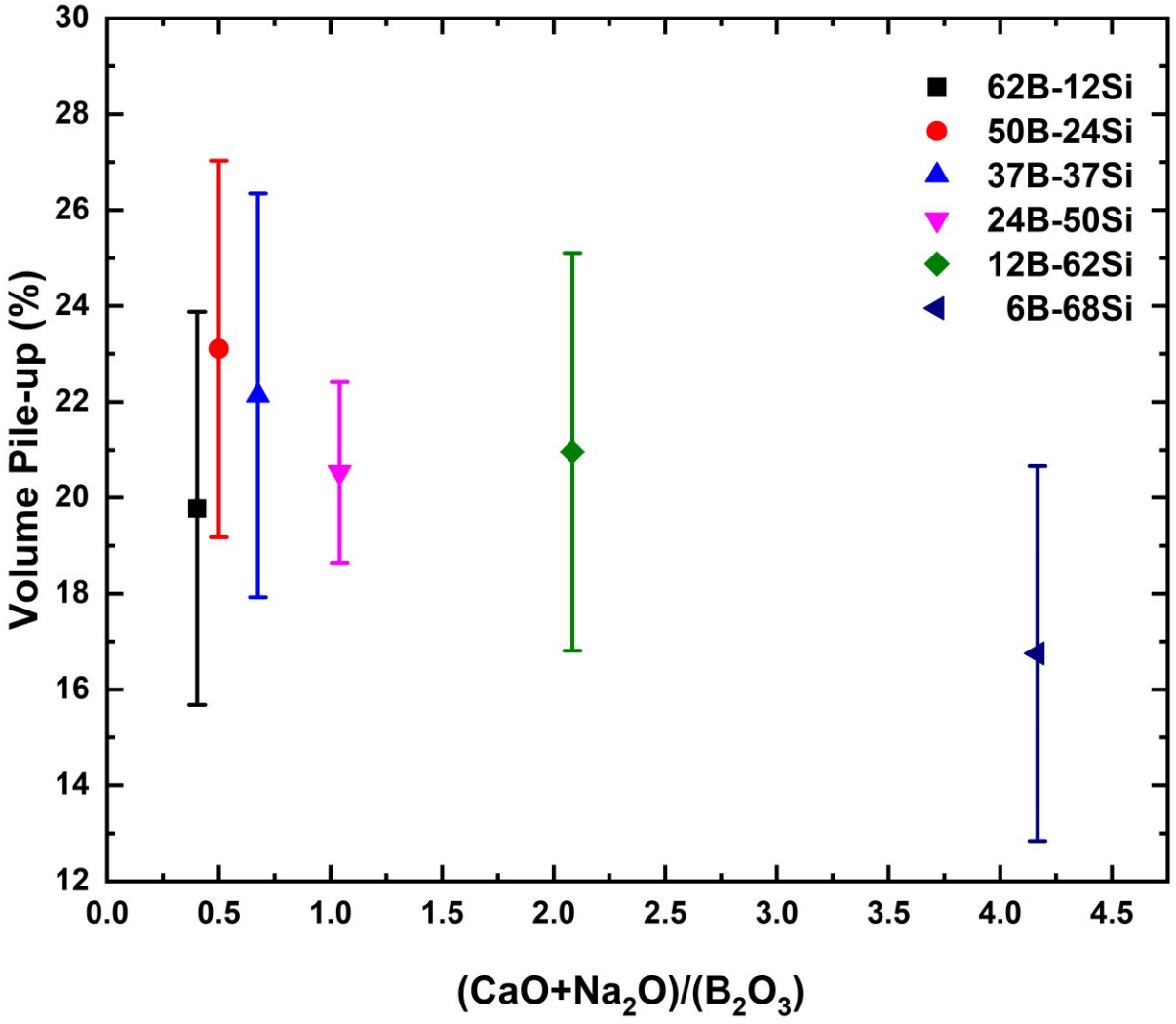

Figure 8. Relation between the fractional volume pileup (V_P) and the network modifiers to boron molar ratio (R value).

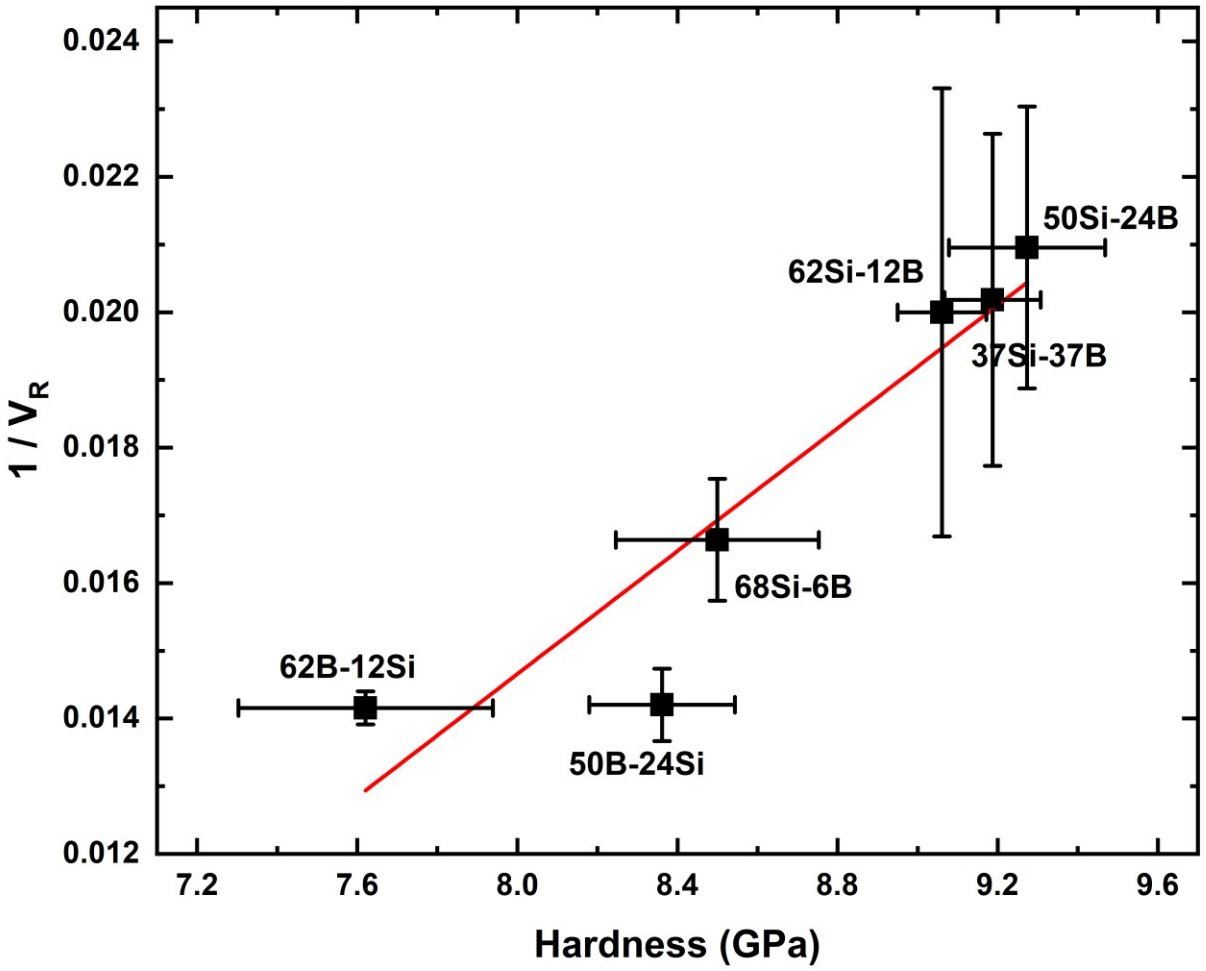

Figure 9. Variation of the inverse of volume recovery (V_R) with respect to hardness.

TABLES

Table 1: Experimental glass composition in mol % and other properties [1].

Glass (ID)	SiO_2	B_2O_3	Na_2O	CaO	T_g (K)	N^4(at%)	Q^4(at%)
62B-12Si	12.7	62.0	14.9	10.4	790	45.3	27
50B-24Si	24.9	49.3	15.0	10.8	803	48.9	33
37B-37Si	36.9	38.4	14.1	10.6	813	53.5	28
24B-50Si	51.6	21.9	15.5	11.0	833	65.5	37
12B-62Si	63.8	10.8	14.8	10.6	842	75.8	31
6B-68Si	69.3	4.9	16.1	9.8	837	80.8	26

Table 2: Experimental values of nominal mean diagonal length (d_i), indentation depth (h_i), volume below (V_i^-) and above (V_i^+), % indentation pile-up (V_i^+ / V_i^-) obtained from AFM images of the various borosilicate glasses indented using Vickers geometry before annealing.

Glass Sample (ID)	Mean Diagonal length (d_i) (µm)		Indentation Depth (h_i) (µm)		V_i^+ (µm^3)	V_i^- (µm^3)	V_i^+/V_i^- %	
	Mean	**S.D.**	**Mean**	**S.D.**	**Mean**	**Mean**	**Mean**	**S.D.**
62B-12Si	5.19	0.13	300.1	8.79	0.180	1.044	17.26	2.37
50B-24Si	5.02	0.12	266.72	3.18	0.160	0.820	18.52	1.48
37B-37Si	4.95	0.08	275.05	7.21	0.142	0.927	15.68	2.96
50Si-24B	4.91	0.13	273.58	8.16	0.150	0.935	16.28	2.24
62Si-12B	4.92	0.06	277.82	3.18	0.138	0.861	16.38	1.57
68Si-6B	5.01	0.04	292.9	3.01	0.126	0.876	14.55	1.39

Table 3: Experimental values of nominal mean diagonal length (d_a), indentation depth (h_a), volume below (V_a^-) and above (V_a^+), % volume recovery (V_r), % volume pile-up (V_p) obtained from AFM images of the various borosilicate glasses indented using Vickers geometry after annealing.

Glass Sample (ID)	Mean Diagonal length (d_a) (µm)		Indentation Depth (h_a) (µm)		V_a^+ (µm^3)	V_a^- (µm^3)	V_R %		V_P %	
	Mean	**S.D.**	**Mean**	**S.D.**	**Mean**	**Mean**	**Mean**	**S.D.**	**Mean**	**S.D**
62B-12Si	4.28	0.23	158.3	2.91	0.1549	0.2795	70.65	1.22	19.78	4.1
50B-24Si	3.81	0.18	139.3	3.39	0.1134	0.2025	70.50	2.65	23.1	3.92
37B-37Si	4.86	0.10	172.3	2.84	0.0864	0.4212	50.29	6.1	22.13	4.21
50Si-24B	4.71	0.13	179.2	9.38	0.1121	0.4454	48.19	4.79	20.52	1.88
62Si-12B	4.74	0.08	180.5	10.7	0.1119	0.4191	51.40	8.50	20.95	4.14
68Si-6B	4.72	0.08	172.17	4.74	0.1085	0.3283	60.27	3.25	16.74	3.91